

The Near-Infrared Extinction Law in Regions of High A_V

T. J. T. Moore¹ S. L. Lumsden² N. A. Ridge³ P. J. Puxley⁴

¹*Astrophysics Research Institute, Liverpool John Moores University, Twelve Quays House, Egerton Wharf, Birkenhead, CH41 1LD, UK.*

²*Department of Physics and Astronomy, University of Leeds, Leeds LS2 9JT*

⁴*Harvard-Smithsonian Center for Astrophysics, 60 Garden St, Cambridge, MA 02138 USA*

⁵*Gemini Observatory, c/o AURA, Casilla 603, La Serena, Chile*

This is a preprint of an Article accepted for publication in Monthly Notices of the Royal Astronomical Society ©2005 RAS

ABSTRACT

We present a spectroscopic study of the shape of the dust-extinction law between 1.0 and 2.2 μm towards a set of nine ultracompact H II regions with $A_V \gtrsim 15$ mag. We find some evidence that the reddening curve may tend to flatten at higher extinctions, but just over half of the sample has extinction consistent with or close to the average for the interstellar medium. There is no evidence of extinction curves significantly steeper than the standard law, even where water ice is present. Comparing the results to the predictions of a simple extinction model, we suggest that a standard extinction law implies a robust upper limit to the grain-size distribution at around 0.1 – 0.3 μm . Flatter curves are most likely due to changes in this upper limit, although the effects of flattening due to unresolved clumpy extinction cannot be ruled out.

Key words: dust, extinction; H II regions; infrared: ISM

1 INTRODUCTION

Accurate knowledge of the extinction law is crucial to most forms of observational astronomy. A detailed understanding of extinction in the infrared (IR) waveband, as it applies in differing environments, is especially important for the study of any heavily embedded object, from young stars to the cores of starburst galaxies and AGN. The average extinction law in the diffuse interstellar medium is well defined in the near-IR and apparently shows little variation (e.g. Mathis 1990). However, the broad studies which produce this conclusion are based on low-extinction data (e.g. Savage & Mathis 1979 with $A_V \lesssim 2$; Cardelli, Clayton & Mathis 1989 with $A_V \lesssim 5$). There is a little accurate information on how extinction curves might vary along lines of sight to heavily embedded objects. It is this latter question that we are investigating in this paper.

There are many reasons to expect an altered extinction curve in regions of high gas density and at large A_V . Average grain sizes are expected to be higher in sheltered molecular cloud environments than in the diffuse interstellar medium because of the processes of grain coagulation and the growth of icy mantles where $A_V \gtrsim 3$ (Whittet et al. 1983, Tielens 1989). There is now plenty of evidence for significantly altered grain-size distributions and increased average grain sizes in dense molecular clouds and star-formation regions. Such alterations cause variations in the extinction parameter $R = A_V/E(B - V)$ and the wavelength of maximum polarisation by dichroic absorption where the extinction is higher (Savage & Mathis 1979, Whittet et al. 2001). In gen-

eral, the value of R rises from the interstellar average of 3.1 to between 4 and 5 in dark clouds and regions of star formation. Such a change indicates a flattening of the extinction curve at wavelengths shorter than 0.5 μm and is associated with alterations in the population of smaller dust grains (e.g. Cardelli & Clayton 1991).

Additional evidence for grain processing in dense regions comes from, e.g., IR reflection nebulae associated with star formation, in the wavelength dependence of the scattered intensity (Castelaz et al. 1985), the scattering optical depth (Yamashita et al. 1989) and the shape of the 3.09 μm ice absorption feature (Pendleton, Tielens & Werner 1990). All appear to be affected by the presence of significant numbers of large dust grains, and depletion of smaller grains may cause changes in the near-IR continuum extinction in low-mass YSOs (Moore & Emerson 1994).

We have carried out observations of hydrogen recombination lines in a number of compact and ultracompact H II regions, and calculated the extinction law for these objects by comparing the line ratios with the predictions of well-established theoretical models (Hummer & Storey 1995). This method has been used previously by Landini et al. (1984) and Lumsden & Puxley (1996). The latter found that the G45.12+0.13 H II region displays an extinction law somewhat steeper than the standard curve. This paper extends the latter study, looking for evidence of widespread variations from standard extinction towards ultracompact H II regions with $A_V \gtrsim 15$.

Table 1. Targets, observed positions and slit orientations

Object	IRAS name	RA (J2000)	Dec. (J2000)	Distance ^a (kpc)	slit angle ^b
G29.96–0.02	18434–0242	18 46 03.9	–02 39 21.9	6.0	60°
G35.20–1.74	18592+0108	19 01 46.5	+01 13 24.8	3.0	90°
G43.89–0.78	19120+0917	19 14 26.2	+09 22 33.9	9.0	90°
G45.45+0.06	19120+1103	19 14 21.4	+11 09 14.1	4.2/8.8	90°
W51d	19213+1424	19 23 39.9	+14 31 08.3	7.0	121°
RCW 57	11097–6102	11 11 54.0	–61 18 23.9	3.1	90°
G298.23–0.33	12073–6233	12 10 00.9	–62 49 54.5	11.0	90°
G307.57–0.62	13291–6249	13 32 31.2	–63 05 19.8	2.7	90°
G337.95–0.48	16374–4701	16 41 08.1	–47 06 46.7	2.9	90°
He2-117		13 42 36.3	–61 22 26.6	–	90°
He2-96		15 05 59.5	–55 59 18.5	–	90°

^aSee §3.2 for references; ^bEast of north

2 OBSERVATIONS

Observations were made on 18, 19 and 20 May 1997 and 10 and 12 June 1998 with the common-user infrared imaging spectrometer IRIS on the AAT with the cs/36 secondary. Nine HII regions were observed with two planetary nebulae as comparison sources. Standards were observed at similar airmass, and where possible G-type stars were used, as they have few intrinsic absorption features. Where F-type stars had to be used, we interpolated over absorption lines in their spectra.

Observations were made in two modes with IRIS. The main data presented here were obtained using cross-dispersed echelle grisms to obtain complete coverage of *IJ* or *HK* in a single exposure. The slit width was 1.5'' and the slit length 13.6'', with a pixel scale of 0.8'' per pixel. The resolution averaged over the wavelength coverage of each grism is approximately 400. Sky subtraction was achieved through observations of an offset blank sky field after every target observation, with the exceptions of the planetary nebulae, G35.20–1.74 and G43.89–0.78, where the objects were compact enough that it was possible to nod along the slit. Objects were aligned on the slit using the imaging mode. The co-ordinates given in Table 1 represent the mid-point of the object as placed in the slit.

The data were flat-fielded using a tungsten lamp before the appropriate on-off pairs were combined. Corrections for the curvature of the echelle orders were then applied. Finally spectra were extracted in a region covering the peak of the emission and approximately 5 rows either side, or in the cases where sky subtraction was derived from nodding along the slit, spectra were extracted at the peak of the positive and negative images by summing over 3 pixel rows and the two spectra were then subtracted. Wavelength calibration was achieved by means of an argon arc lamp.

The other observing mode used only the single-order H-grism. This gave a resolution of approximately 100 with the cs/36 secondary, and wavelength coverage spanning 1.2–2.1 μ m. These data were acquired to assist in aligning the separate *IJ* and *HK* echelle spectra, since it was found that the poor atmospheric transmission in the region 1.35–1.45 μ m, caused by water and CO₂, made it difficult to join the *IJ* orders to the *HK* orders accurately. The low resolution spectra by comparison give a well defined continuum shape covering wavelengths included by both echelles. These spectra were all acquired during the 1998 observations. The

Table 2. H I recombination-line line fluxes for the two planetary nebula targets, as a percentage relative to F(Br γ)

Line	$\lambda(\text{air})/\mu\text{m}$	He2-96	He2-117	Case B
Pa δ	1.005	81.5 \pm 6.0	56.7 \pm 3.9	201.1
Pa γ	1.095	158 \pm 11	121.2 \pm 8.5	327.6
Pa β	1.282	369 \pm 26	329 \pm 24	589.1
Br16	1.556	5.8 \pm 0.4	5.2 \pm 0.4	8.0
Br15	1.570	7.1 \pm 0.5	6.9 \pm 0.5	9.7
Br14	1.588	9.3 \pm 0.7	9.0 \pm 0.6	11.9
Br13	1.611	12.1 \pm 0.9	10.9 \pm 0.7	14.9
Br11	1.681	19.6 \pm 1.4	18.5 \pm 1.3	24.7
Br10	1.736	29.4 \pm 2.1	27.1 \pm 1.9	33.1
Br γ	2.166	100 \pm 5	100 \pm 5	100.0

same nod patterns were used here as in the echelle observations. Wavelength calibration was by means of identifying the bright Paschen and Brackett lines in the planetary nebulae.

The reduction of the straightened IRIS frames then followed a standard procedure, using the FIGARO data reduction package. The same procedure was applied to the standard-star spectra. Each object spectrum was then divided by its corresponding standard spectrum, and corrected for the black-body shape of the standard.

The numbers of lines detected depends on the brightness of the target, the extinction towards it and the atmospheric seeing. Fluxes for the H I emission lines were obtained by fitting Gaussian functions. Errors are taken from the fit parameters or assumed to be 5%, reflecting the estimated accuracy of continuum matching between spectral bands, whichever is the larger.

3 RESULTS

Figure 1 shows the reduced JHK spectrum of G298.23–0.33 as an example of the data obtained. The separated continuum level has been matched using the low-resolution grism spectrum as described above.

Hydrogen recombination-line flux ratios are given, relative to that of Br γ , in Tables 2 and 3. Table 2 contains results for the two planetary nebulae, observed as low-extinction comparisons to the HII regions. These were acquired to test the accuracy of our observations since they have well defined optical extinction values. Table 3 contains the main

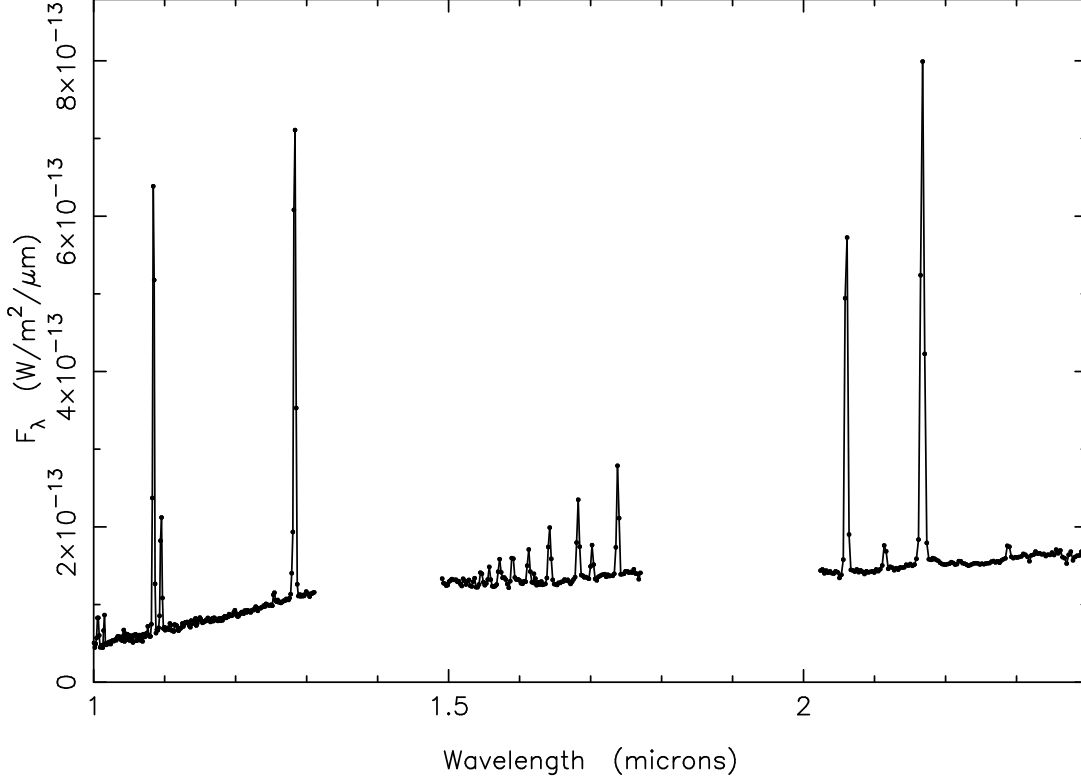


Figure 1. The reduced 1.0 – 2.8- μm spectrum of G298.23–0.33 containing lines of the Paschen and Brackett series of hydrogen. The three sections have been matched using a low-resolution grism spectrum as a template (see §2).

Table 3. Measured hydrogen recombination-line fluxes for the H II regions, as a percentage relative to $F(\text{Br}\gamma)$.

Line	G29.96–0.02	G35.20–1.74	G43.89–0.78	G45.45+0.06	W51d	RCW 57	G298.23–0.33	G307.57–0.62	G337.95–0.48
Pa δ	–	–	–	–	–	14.0 ± 1.0	3.1 ± 0.2	–	–
Pa γ	1.03 ± 0.07	–	–	–	3.77 ± 0.26	40.2 ± 2.8	10.7 ± 0.7	9.5 ± 0.7	2.7 ± 0.2
Pa β	16.3 ± 1.1	14.6 ± 1.0	14.2 ± 1.6	11.4 ± 1.3	32.9 ± 2.3	127 ± 9	58.1 ± 4.1	53.9 ± 3.8	20.6 ± 1.4
Br16	1.02 ± 0.07	1.02 ± 0.07	–	–	1.92 ± 0.13	–	–	–	–
Br15	1.30 ± 0.10	1.18 ± 0.08	–	–	2.43 ± 0.17	–	3.8 ± 0.3	–	–
Br14	2.10 ± 0.15	1.75 ± 0.12	–	–	3.87 ± 0.27	6.36 ± 0.83	3.9 ± 0.5	–	–
Br13	2.81 ± 0.19	2.49 ± 0.17	–	–	3.85 ± 0.27	6.8 ± 1.0	4.6 ± 0.3	–	–
Br11	7.78 ± 0.53	5.57 ± 0.39	5.45 ± 0.38	6.46 ± 0.45	8.53 ± 0.60	13.7 ± 1.1	10.9 ± 0.8	10.1 ± 0.8	7.4 ± 0.5
Br10	13.06 ± 0.88	–	6.57 ± 0.46	7.00 ± 0.50	11.6 ± 0.8	20.0 ± 1.4	14.5 ± 1.0	17.9 ± 1.3	9.5 ± 0.7
Br γ	100 ± 5	100 ± 5	100 ± 5	100 ± 5	100 ± 5	100 ± 5	100 ± 5	100 ± 5	100 ± 5

results for the HII regions. The results are shown graphically in Figures 2 and 3 for the HII regions and planetary nebulae, respectively. The Br12 line at $1.641 \mu\text{m}$ has been excluded from all fits and calculations since it is blended in these observations with the [FeII] $1.644 \mu\text{m}$ line.

Observed line ratios are compared to predicted values from the models of Hummer & Storey (1995) with $n_e = 10^4 \text{ cm}^{-3}$ and $T_e = 10^4 \text{ K}$. Following Landini et al. (1984), if the wavelength dependence of the dust opacity is assumed to follow a power law, so that $\kappa(\lambda) \propto \lambda^{-\alpha}$, then the differential optical depth between two lines, measured as

$$\Delta\tau_{12} = -\ln \frac{[I(\lambda_2)/I(\lambda_1)]_{\text{obs}}}{[I(\lambda_2)/I(\lambda_1)]_{\text{theory}}},$$

is equivalent to

$$\Delta\tau_{12} = \tau_{\lambda_1} [(\lambda_2/\lambda_1)^{-\alpha} - 1],$$

and the parameters τ_{λ_1} and α can be fitted to the data, in this case, by minimising χ^2 using the Marquardt method (Fortran routine MRQMIN from Press et al. 1993). We have taken $\lambda_1 = \lambda(\text{Br}\gamma) = 2.166 \mu\text{m}$ as the reference wavelength in all cases. The results of these fits are listed in Table 4 and plotted in Figures 2 and 3.

3.1 General Results

Figure 4 shows the compiled results from fitting power-law extinction curves to the data. Also plotted is the result for G45.12+0.13 obtained by Lumsden & Puxley (1996). Four objects have α values more than 2σ below the mean inter-

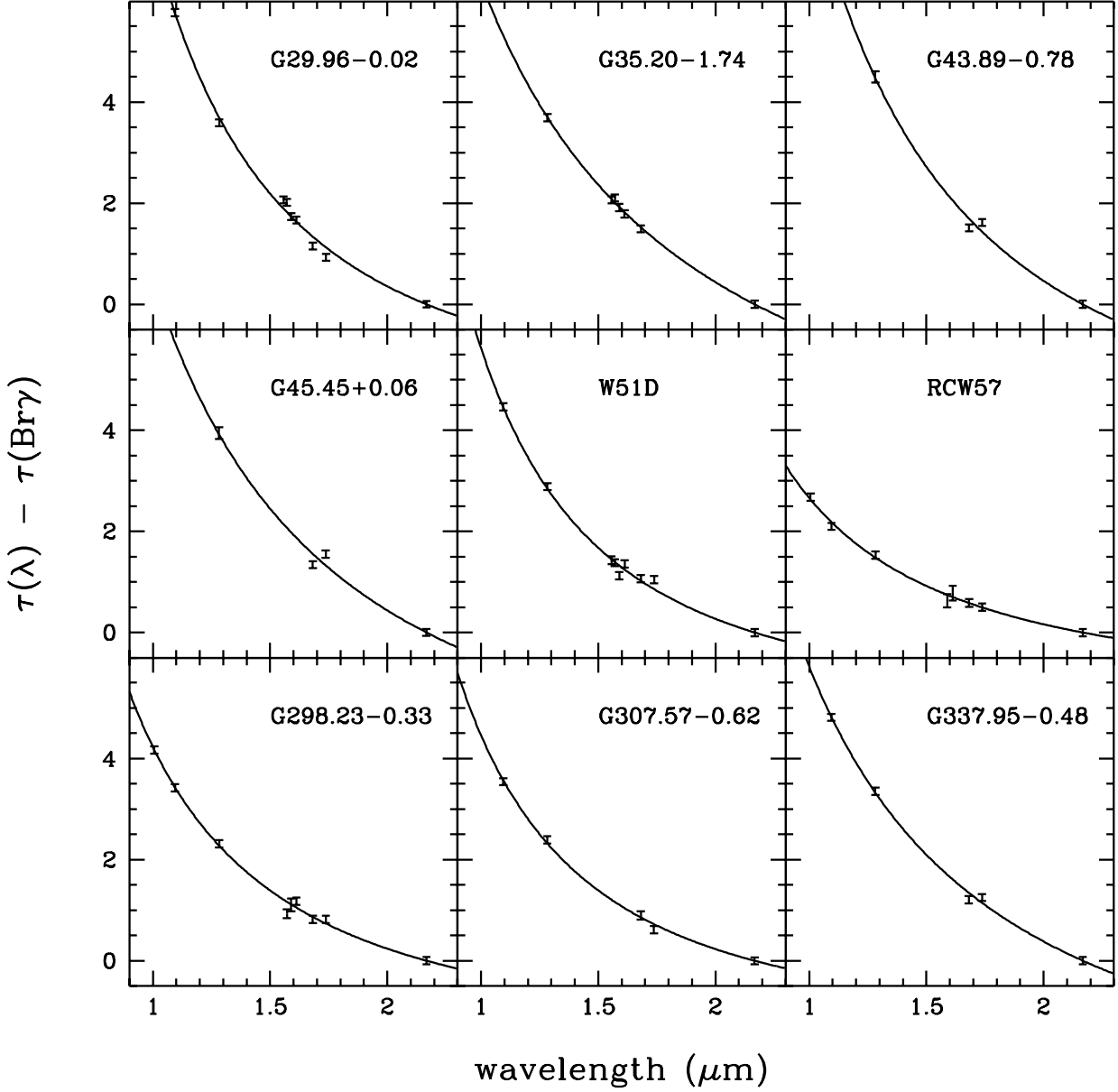


Figure 2. Extinction-law fits to the HII-region recombination-line data.

Table 4. Extinction-law fit parameters

Source	α	$\tau(\text{Br}\gamma)$	χ^2_{red}	τ_{10}^a
G29.96-0.02	1.90 ± 0.05	6.16 ± 0.07	4.71	1.2
G35.20-1.74	1.11 ± 0.12	4.68 ± 0.23	0.48	4.6
G43.89-0.78	1.63 ± 0.14	3.32 ± 0.21	6.5	2.8
G45.45+0.06	1.33 ± 0.16	3.89 ± 0.26	10	2.7
W51d	1.95 ± 0.07	1.59 ± 0.07	2.57	1.7
RCW 57	1.39 ± 0.14	1.38 ± 0.13	0.57	1.7
G298.23-0.33	1.59 ± 0.08	1.76 ± 0.09	1.86	1.7
G307.57-0.62	1.79 ± 0.14	1.50 ± 0.13	1.3	2.3
G337.95-0.48	1.23 ± 0.09	3.67 ± 0.20	1.9	2.5
He2-96	1.93 ± 0.32	0.27 ± 0.06	0.49	–
He2-117	1.71 ± 0.23	0.46 ± 0.07	0.53	–

^aSee §4

stellar value of 1.8 (e.g. Martin & Whittet 1990) and three of these are the three objects with largest fitted values of $\tau(\text{Br}\gamma)$. None of the current targets has α significantly larger than 1.8.

The nine HII regions have 10- μm silicate optical depths (τ_{10}) estimated by Simpson & Rubin (1990; hereafter SR) or Faison et al. (1998), from fits to low-resolution spectra. This gives us an independent check of the apparent trend in Figure 4. Figure 5(a) shows α plotted against these, taking the lower of the τ_{10} values obtained by SR. Figure 5(b) shows our fitted values of $\tau(\text{Br}\gamma)$ plotted against τ_{10} .

Five objects have τ_{10} values and independent A_V estimates available in the literature. These suggest that $A_V \sim 10\tau_{10}$ and so τ_{10} should be comparable in size to the optical depth at the wavelength of $\text{Br}\gamma$.

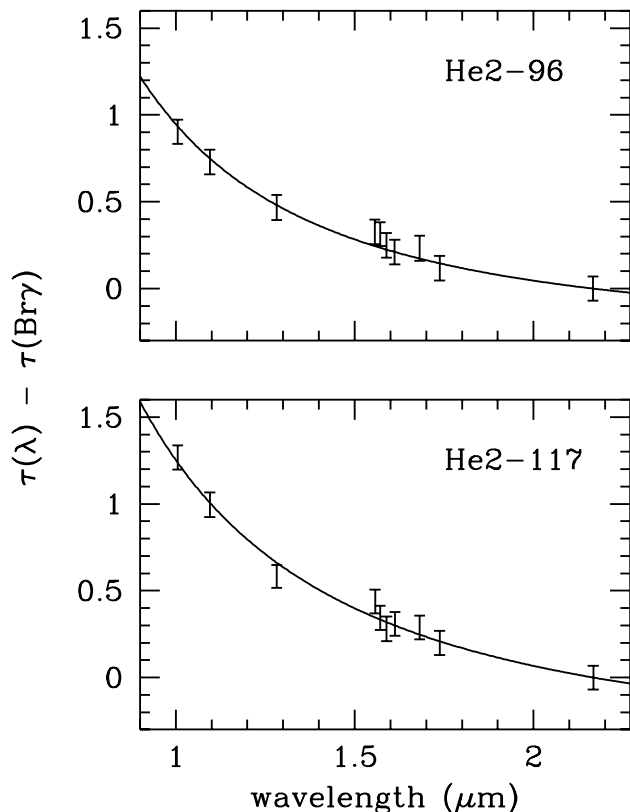


Figure 3. Extinction-law fits to data for the PN He2-96 and He2-117. The numerical results are given in Table 2.

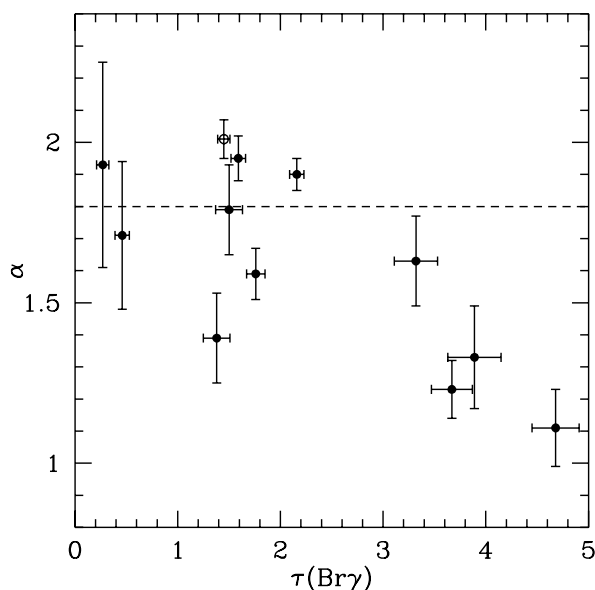


Figure 4. Extinction-law fit parameters α (the power-law exponent) against the continuum optical depth at Br γ . The dashed line represents $\alpha = 1.8$ the mean exponent for the general interstellar medium (Martin & Whittet 1990). The open point represents the result for G45.12+0.13 found by Lumsden & Puxley (1996).

3.2 Notes on individual objects

G29.96-0.02 This object has a likely distance of 6 kpc (Pratap, Megeath & Bergin 1999). Peeters et al. (2002) report no detection of 3.1- μm water-ice absorption in ISO data. Estimates of extinction are $A_K = 2.14 \pm 0.08$ (Watson et al. 1997), $A_K = 1.6$ and $A_H = 3.6$ (Morisset et al. 2002). Herter et al. (1981) estimate $\tau_{10} = 1.9 \pm 0.4$. Faison et al. (1998) modelled $\tau(2.2) = 1.9$ and $\tau_{10} = 1.2$. Our fit produces a $\tau(\text{Br}\gamma)$ consistent with most of these, and α about 2σ steeper than the standard value of 1.8.

G35.20-1.74 At a distance of 3 kpc (Chan, Henning & Schreyer 1996), this source has $A_V > 22$ mag (Woodward, Helfer & Pipher 1985). Our fitted $\tau(\text{Br}\gamma)$ is about twice the value extrapolated from this limit using a standard extinction law, and is therefore also consistent with the very flat curve we derive ($5-6\sigma$ below the mean interstellar slope). Faison et al. (1998) model $\tau(2.2) = 4.1$ and $\tau_{10} = 4.6$. The 3.1- μm water-ice feature has been detected (paper in preparation).

G43.89-0.78 The estimated distance for this object is 9 kpc and $\tau_{10} = 2.8$ (SR). Our fitted extinction curve is consistent with the standard law.

G45.45+0.06 $D = 4.2$ or 8.8 kpc (Chan et al. 1996) and $\tau_{10} = 2.7$ (SR). The mean $A_K \simeq 2.5$ across the H II region, with a peak $A_K = 3.6$ (with corresponding A_V values of 23 and 33; Feldt et al. 1998). Our $\tau(\text{Br}\gamma)$ is consistent with the latter and α is about 3σ flatter than the mean extinction law.

W51d The most luminous component of the giant H II region W51, at a distance of 7.0 kpc (Takahashi et al. 2000). $A_V = 24 \pm 3$ was determined by Goldader & Wynn-Williams (1994). Faison et al. (1998) modelled $\tau(2.2) = 2.6$ and $\tau_{10} = 1.7$. Our value for α is 2σ larger than the standard law.

RCW 57 (G291.3-0.7) from the catalogue of Rodgers, Campbell & Whiteoak (1960). Its distance is given as 3.1 kpc (SR). Persson, Frogel & Aaronson (1976) determined $A_V = 15$ and SR found a silicate optical depth of $\tau_{10} = 1.7$ (but see §4). Our fit produces a value of $\tau(\text{Br}\gamma)$ consistent with these and a rather flat α (3σ below 1.8). Pandey & Ogura (1998) find $R = 4.4$ towards the NGC 3603 cluster, indicating that the extinction curve is also flatter than the average at visible wavelengths.

G298.23-0.33 This object has estimated distance ~ 11 kpc (Chan et al. 1996), $A_V \simeq 14$ (Persson et al. 1976) and $A_K = 0.8$ (Martín-Hernández et al. 2002). $\tau_{10} = 1.7$ (SR) but H₂O ice is not detected (Peeters et al. 2002). Our fitted α is flatter than the interstellar mean by about 2σ . $\tau(\text{Br}\gamma)$ is about twice the above A_K value, but is more consistent with A_V and τ_{10} .

G307.57-0.62 The distance estimate is 2.7 kpc (Chan et al. 1996) for this source and $\tau_{10} = 2.3$ (SR). Our fitted extinction law is consistent with the standard interstellar value.

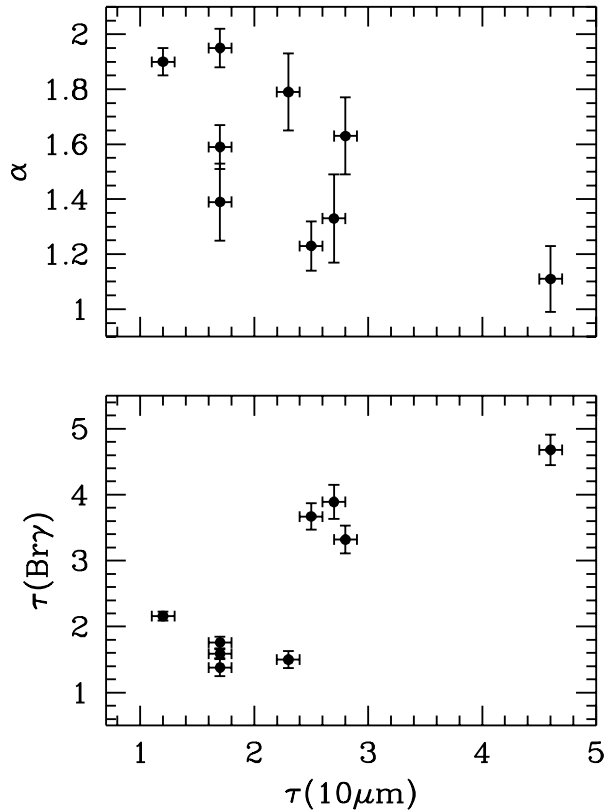


Figure 5. (a) fitted values of α (the extinction-law exponent) against the optical depth in the silicate feature τ_{10} listed by Simpson & Rubin (1990) and Faison et al. (1998); (b) fitted $\tau(\text{Br}\gamma)$ values against τ_{10} . Uncertainties in τ_{10} are taken to be 0.1 in each case.

G337.95–0.48 SR give $D = 2.9$ kpc and $\tau_{10} = 2.5$ for this object. Our spectra were taken during a period of very poor seeing which has resulted in only a few of the Brackett series lines being measured. The estimate of α we obtain is significantly (6σ) below the canonical value.

Planetary Nebulae He2-96, He2-117 The derived extinction law for these objects is consistent with the mean ISM law, although the error bars on our fits are large. These objects have measured Balmer decrements of ~ 2.0 (He2-96) and 2.7 (He2-117) (Tylenda et al. 1992). Assuming the standard extinction law, these values correspond to $\tau(\text{Br}\gamma) = 0.33$ and 0.44, respectively, consistent with our fitted values (Table 4).

4 DISCUSSION

Figure 4 suggests an upper boundary to α and an increased probability that objects with higher absolute extinction ($\tau(\text{Br}\gamma) \gtrsim 2.5$ or $A_V \gtrsim 25$) will have $1\mu\text{m} - 2\mu\text{m}$ extinction curves that are flatter than the mean interstellar law. The data (including the PN and G45.12+0.13 points) have a Spearman rank correlation coefficient of $r_s = -0.636$ which has an associated probability of arising at random of

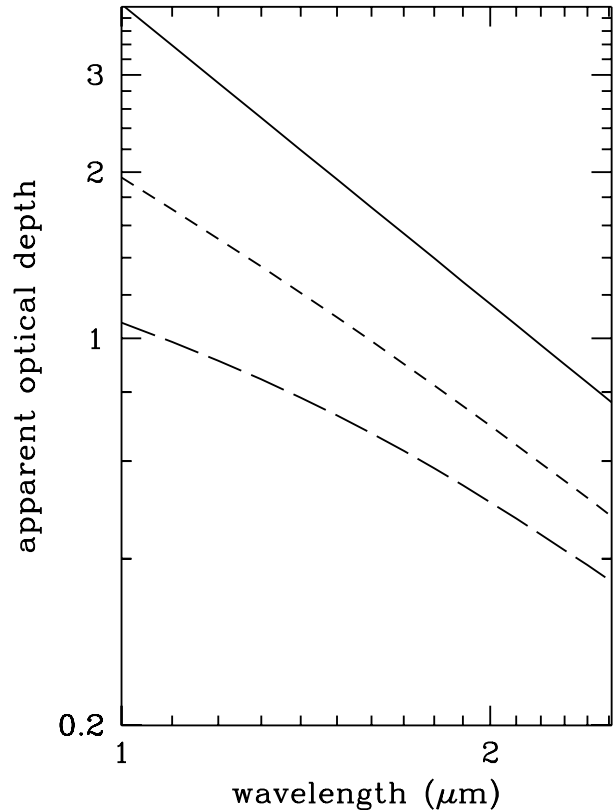


Figure 6. A simple two-component model to demonstrate the apparent flattening of the measured extinction law caused by unresolved optical depth structure. Here, there are two sources in the beam with optical depth ratios of 1.0 (solid line), 3 (short dashed) and 10 (long dashed).

2.6×10^{-2} for $N = 12$. This result lends support to the tentative report of flattened extinction for $A_V \gtrsim 15$ by Kenyon, Lada & Barsony (1998), from a statistical analysis of photometric data in ρ Oph. It also supports the finding of Racca et al. (2002) that flatter near-IR extinction laws are found where higher extinction regions are present.

Figure 5(a) shows an apparently similar distribution of α with $10\text{-}\mu\text{m}$ silicate-absorption optical depth obtained by fits to *IRAS* LRS data (SR) and to low-resolution ($R = 60$) spectroscopy (Faison et al. 1998). Figure 5(b) shows that our fitted optical depths vary more or less as expected with τ_{10} , although the significance of the correlation is not high (the probability of it arising at random is 3.8 per cent). A least-squares fit gives a gradient of 1.0 ± 0.3 and intercept 0.3 ± 0.7 . The large scatter should not be too surprising, since there may be large uncertainties in τ_{10} in these low-resolution spectra, due to PAH emission features on either side of it. There may also be silicate emission components filling in the absorption feature (Aitken 1996) and significant positional and beam-size discrepancies with our near-IR observations.

Figure 4 also shows that one target (RCW 57) has a low fitted value of α without having a particularly high extinction. It should be noted, however, that there are large amounts of extended, structured emission (e.g. 2MASS K_s

images) in this target and that it contains a cluster of objects, some of which have localised high extinction (e.g. $\tau_{10} = 3.7$ or $A_V = 59$, Barbosa et al. 2003) close by our observed position.

There are two main potential causes of flatter observed extinction curves. One is unresolved optical depth structure, the other is a physical change in the dust grain properties, especially the size distribution, in the material around the source. These are discussed below.

4.1 Structure within the beam

Figure 6 shows the results of a simple two-component model to demonstrate the effects of extinction structure within the beam. Three cases are shown in which the wavelength-dependence of the extinction is $\tau(\lambda) \propto \lambda^{-1.8}$ for both components, but where optical depths at $2.166 \mu\text{m}$ are in the ratios 1.0, 3.0 and 10.0. It can be seen that the apparent extinction curve becomes flatter with increasing contrast in the unresolved optical-depth structure, as well as departing from a single power law. Single power-law fits to the latter two cases would produce exponents close to 1.5 and 1.2, respectively. The cause of this artificial flattening is the penetration of short-wavelength emission through the regions of low extinction.

As mentioned above, at least one HII region with a low fitted α value (RCW 57) is associated with large amounts of extended structure. However, there are two reasons to think that the effects of unresolved structure may not be the principal cause of the flatter extinction curves. The first comes from the model, which shows that the extinction contrast has to be large to produce curves as flat as some of those observed. Secondly, we might expect that more distant sources have more unresolved structure and therefore tend to have flatter extinction curves, but we find no correlation between fitted α values and source distance. We should, therefore examine the effect of variable dust-grain properties.

4.2 Grain properties

A simple model of extinction by spherical grains with a size distribution similar to that deduced by Mathis, Rumpl and Nordsieck (1977; MRN) can be used to place rough constraints on the grain-size distribution in these regions. We have calculated the opacity of an equal-abundance mix of silicate and graphite grains using the Mie scattering code BHMIE by Bohren & Huffman (1983) and the optical constants used by Weingartner & Draine (2001). We find that changes in the population of smaller grains, as manifested in a variable minimum grain radius a_{\min} to the MRN-like distribution ($n(a) \propto a^{-3.5}$), does not affect the slope of the near-IR extinction curve between $1 \mu\text{m}$ and $2 \mu\text{m}$ (Figure 7). The shape of the curve is much more sensitive to the maximum grain radius a_{\max} and becomes flatter both when a_{\max} is small (because the absence of larger grains means that absorption becomes a more important component of the extinction) and when a_{\max} is large (when scattering by the larger grains is no longer in the Rayleigh regime). Larger grains are the more likely case here, since there is other evidence of grain growth in star-formation regions (see Introduction).

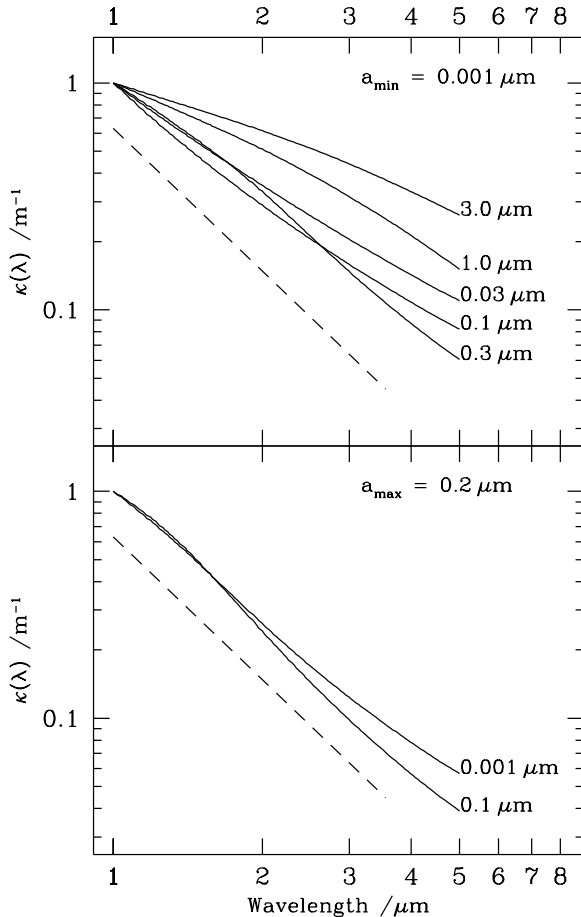


Figure 7. Results of simple Mie-scattering model of the near-IR extinction opacity due to spherical grains with a size distribution $n(a) \propto \lambda^{-3.5}$. (a) shows the effect of increasing the maximum grain size; (b) shows the that there is little effect in altering the minimum grain size. The dashed line represents a power law of $\lambda^{-1.8}$. All models curves are normalised to 1 at $\lambda = 1.0 \mu\text{m}$.

These simple models suggest that it is not easy to obtain a near-IR extinction law that is significantly steeper than the empirical power law ($\tau \propto \lambda^{-\alpha}$, $\alpha \simeq 1.8$). A steeper slope would require a large proportion of weakly absorbing grains in the mix. Thick mantles of pure water ice (depth $\gtrsim 0.1 \mu\text{m}$) would have this effect, creating a steep extinction curve out to the edges of the strong $3.1\text{-}\mu\text{m}$ feature (ignoring the weak features at $\sim 1.5 \mu\text{m}$ and $\sim 2 \mu\text{m}$). Water ice exists toward one source in our list (G35.20-1.74, section 3.2) but, given that steep curves are not found, the mantles must be relatively thin (significantly less than $0.1 \mu\text{m}$ thick).

The model results also imply that reproduction of the standard extinction-law exponent, especially at wavelengths between $1 \mu\text{m}$ and $2 \mu\text{m}$, requires values of a_{\max} to be between $0.1 \mu\text{m}$ and $0.3 \mu\text{m}$ (Fig. 7). Physically, this limit may arise from the balance between grain coagulation and destruction processes. Departures from it are more likely where there is high line-of-sight extinction, but this is not the only variable (local density and temperature should be involved).

There was little effect on the model predictions from introducing increases in the silicate fraction, the addition

of amorphous carbon or fluffy composite grains, or from changes in the slope of the size distribution.

Our results are quite consistent with the predictions of the model of Krügel & Siebenmorgen (1994). These authors also predict no significant change of slope of the extinction curve between wavelengths of 1 and $2\mu\text{m}$ for grains with a size distribution upper limit of $0.3\mu\text{m}$, applicable to dust in a dense molecular cloud. (see their Figure 12). An observable flattening of the extinction law is predicted by their models for grain distributions with upper limits $> 0.3\mu\text{m}$. Other studies that fit grain models to normal extinction also predict upper limits to the grain radius in a narrow range close to $0.2\mu\text{m}$ (e.g. Weingartner & Draine 2001).

5 CONCLUSIONS

Determinations of the extinction law between $1\mu\text{m}$ and $2\mu\text{m}$ have been made towards nine ultracompact HII regions with $A_V \gtrsim 15$, using HI line ratios. Four objects have power-law fits $\tau \propto \lambda^{-\alpha}$ with fitted values of α more than 2σ lower than the average interstellar value of 1.8. None of the targets shows a significantly steeper extinction law. There is an apparent trend for the sources with highest extinction to have flatter extinction curves but low values of α are found at all extinctions. Although unresolved clumpy extinction structure can cause apparent flattening of the extinction law, the observed shallow curves are likely to be due to changes in the dust properties. We will examine this trend further in Paper II where we study the extinction law from $2\text{--}5\mu\text{m}$ in a sample of HII regions with average extinction higher than those presented here. A simple scattering model shows that changes to the maximum grain radius in high column density regions are the most likely cause and that the canonical $\alpha = 1.8$ exponent suggests that the maximum grain size is tightly constrained to be close to $0.2\mu\text{m}$. This upper limit must be the result of balance between grain destruction and coagulation processes. Any significant change to the maximum grain radius due to a change in this balance will cause a flattening of the near-IR extinction curve.

ACKNOWLEDGMENTS

We thank the staff of the Anglo-Australian Observatory for their support and the anonymous referee for helpful comments on the manuscript.

REFERENCES

- Aitken D. K., 1996, in: Roberge W. G., Whittet, D. C. B., eds, ASP Conf., Ser. Vol. 97, Polarimetry of the Interstellar Medium, Astron. Soc. Pac. San Francisco p. 225
- Bohren C. F., Huffman D. R., 1983, *Absorption and Scattering of Light by Small Particles*, Wiley.
- Cardelli J. A., Clayton G. C., 1991, *AJ*, 101, 1021
- Cardelli J. A., Clayton G. C., Mathis, J. S., 1989, *ApJ*, 345, 245
- Castelaz M. W., Hackwell J. A., Grasdalen G.L., Gehrz R.D., Gullixson C., 1985, *ApJ*, 290, 261
- Chan S. J., Henning T., Schreyer K., 1996, *A&AS*, 115, 285
- Faison M., Churchwell E., Hofner P., Hackwell J., Lynch D. K., Russell, R.W., 1998, *ApJ*, 500, 280
- Feldt M., Stecklum B., Henning Th., Hayward T. L., Lehmann Th., Klein R., 1998, *A&A*, 339, 759
- Goldader, J. D., Wynn-Williams C. G., 1994, *ApJ*, 433, 164
- Herter T., Helfer H. L., Forrest W. J., McCarthy J., Houck J. R., Willner S. P., Puetter R. C., Rudy R. J., Soifer B. T., Pipher J. L., 1981, *ApJ*, 250, 186
- Hummer D. G., Storey P. J., 1995, *MNRAS*, 272, 41
- Kenyon S. J., Lada E. A., Barsony M., 1998, *AJ*, 115, 252
- Kurtz S., Churchwell E., Wood D. O. S., 1994, *ApJS*, 91, 659
- Krügel E., Siebenmorgen R., 1994, *A&A* 288, 929
- Landini M., Natta A., Oliva E., Salinari P., Moorwood A. F. M., 1984, *A&A*, 134, 284, L84
- Lumsden S. L., Puxley P. J., 1996, *MNRAS*, 281, 493
- Martin P.G., Whittet D. C. B., 1990, *ApJ*, 357, 113
- Martín-Hernández, N. L., et al. 2002, *A&A*, 381, 606
- Mathis J. S., 1990, *ARA&A*, 28, 37.
- Mathis J. S., Ruml W., Nordsieck K. H., 1977, *ApJ*, 217, 425
- Moore T. J. T., Emerson J. P., 1994, *MNRAS*, 271, 243
- Morisset C., Schaerer D., Martín-Hernández N. L., Peeters E., Damour F., Baluteau, J.-P., Cox P., Roelfsema P., 2002, *A&A*, 386, 558
- Pandey A. K., Ogura K., 1998, *Bull. Astron. Soc. India*, 26, 545.
- Peeters E., Martín-Hernández N. L., Damour F., Cox P., Roelfsema P., Baluteau, J.-P., Tielens A. G. G. M., Churchwell E., Kessler, M. F., Mathis, J. S., Morisset C., Schaerer D., 2002, *A&A*, 381, 571
- Pendleton Y., Tielens A. G. G. M., Werner M. W., 1990, *ApJ*, 349, 107.
- Persson S. E., Frogel J. A., Aaronson M., 1976, *ApJ*, 208, 753
- Pratap P., Megeath S. T., Bergin E. A., 1999, *ApJ*, 517, 799
- Press W. H., Flannery B. P., Teukolsky S. A., Vetterling W. T., 1993, *Numerical Recipes in FORTRAN 77*, CUP
- Racca G., Gómez M., Kenyon S. J., 2002, *AJ*, 124, 2178
- Rodgers A. W., Campbell, C. T., Whiteoak J. B., 1960, *MNRAS*, 121, 103.
- Savage B. B., Mathis J. S., 1979, *Ann. Rev. Astr. Ap.*, 17, 73.
- Simpson J. P., Rubin R. H., 1990, *ApJ*, 354, 165 (SR).
- Takahashi H., Matsuhara H., Watarai H., Matsumoto T., 2000, *ApJ*, 541, 779
- Tielens A. G. G. M., 1989, *IAU Symp* 135 (Interstellar Dust), p 239.
- Tylenda R., Acker A., Stenholm B., Koeppen J., 1992, *A&AS*, 95, 337.
- Watson A. M., Coil A. L., Shepherd D. S., Hofner P., Churchwell, E., 1997 *ApJ*, 487, 818
- Weingartner, J. C. & Draine B. T., 2001, *ApJ*, 548, 296.
- Whittet D. C. B., Bode, M. F., Longmore, A. J., Baines, D. W. T. & Evans, A., 1983, *Nature* 303, 218.
- Whittet D. C. D., Gerakines, P. A., Hough, J. H., Shenoy, S. S., 2001, *ApJ* 547, 872.
- Wood D. O. S., Churchwell E., 1989, *ApJSS*, 69, 831.
- Woodward C. E., Helfer H. L., Pipher J. L., 1985, *A&A*, 147, 84.

Yamashita T., Sato S., Nagata T., Gatley I., Hayashi S.S.,
Fukui Y., 1989, ApJ, 336, 832.